Angle-resolved photoemission study of $SrTiO_3$ (100) and (110) surfaces

Y. Haruyama and S. Kodaira
Institute of Physics, University of Tsukuba, Tsukuba, Ibaraki 305, Japan

Y. Aiura, H. Bando, and Y. Nishihara
Electrotechnical Laboratory, Tsukuba, Ibaraki 305, Japan

T. Maruyama
Institute of Materials Science, University of Tsukuba, Tsukuba, Ibaraki 305, Japan

Y. Sakisaka
Department of Physics, Faculty of Science, Hirosaki University, Hirosaki, Aomori 036, Japan

H. Kato
Photon Factory, National Laboratory for High Energy Physics, Tsukuba, Ibaraki 305, Japan
(Received 25 May 1995)

Angle-resolved photoemission spectra of $SrTiO_3$ (100) and (110) surfaces have been obtained. The normal-emission data are analyzed using the direct transition model and, as a result, the valence band is determined along the Δ and Σ lines in the bulk Brillouin zone. The empirical valence-band structure is found to be consistent with the band calculations if and only if proper magnitude of the O $2p$ crystal-field splitting is adopted. The effect of the O $2p$ crystal-field splitting on the band structure is discussed.

I. INTRODUCTION

$SrTiO_3$ (cubic perovskite-type structure at room temperature) is a typical insulator with a wide band gap ($\sim$3.2 eV).[1] The bulk electronic density of states (DOS) has been intensively investigated by means of photoemission and bremsstrahlung isochromat spectroscopies.[2–4] In addition, a number of theoretical studies of the electronic structure have been performed using various methods,[5–9] and these theoretical DOS's have often been compared with experimental ones.

Angle-resolved photoemission (ARP) spectroscopy has been used for many metals and semiconductors of low Miller-index faces in order to elucidate their electronic band structure.[10] Recently, this method has also been extended to transition-metal oxides, for example TiO_2,[11] Fe_3O_4,[12] CoO,[13] and NiO,[13,14] and has given us useful information about their electronic structure. So far there is only one report on the band structure of $SrTiO_3$ obtained from the analysis of normal-emission ARP spectra.[15] In the report, however, the band structure was investigated for only a half of the bulk Brillouin zone along the Δ line near the X point. Therefore, essential information about the band structure of $SrTiO_3$, such as the energy position at the Γ point and the width of each band, is still not clear.

In this work, we carried out ARP studies of $SrTiO_3$ (100) and (110) surfaces in order to elucidate the whole band structure along the Γ-Δ-X and Γ-Σ-M lines. The empirical band structure determined from an analysis of the ARP spectra is found to be qualitatively in overall agreement with the band calculations, if the proper magnitude of the O $2p$ crystal-field splitting is adopted. We will discuss the influence of the O $2p$ crystal-field splitting on the band structure.

II. EXPERIMENT

The ARP experiments were performed at the Photon Factory (Beam Lines 11C and 11D), National Laboratory for High Energy Physics. The ARP spectra were measured using the hemispherical electrostatic analyzer with an acceptance angle of $\pm 1°$ [Vacuum Science Workshop (VSW)]. The total instrumental energy resolution was 150–250-meV full width at half maximum, depending on the photon energy ($h\nu$) in the energy range 17–36 eV. All ARP spectra were recorded on normal emission with a light incidence angle of $\theta_i = 50°$ and measured at room temperature. The base pressure in the ARP systems was $\sim 3\times 10^{-10}$ Torr. A Pt foil and a Ta plate (sample holder) in electrical contact with the sample provided the Fermi-energy (E_F) reference.

Polished (100)- and (110)-oriented plate-shaped single crystals of $SrTiO_3$ sample ($8\times 5\times 0.5$ mm^3) were purchased from Earth-Jewelry Co. (Kobe Japan). Samples, which were reduced by annealing in ultrahigh vacuum (UHV) at 800 °C for several hours, were free from the charging effect. Annealing in UHV and O_2, and Ar-ion bombardment at 0.5 keV (current density $\sim 3\times 10^{-7}$ A/cm^2), were used to remove contamination. The cleanliness of the sample surfaces was confirmed by Auger electron and ARP spectroscopies for the absence of extra features arising from contamination. The sample geometrical structure was checked using low-energy electron diffraction for both (100) and (110) surfaces.

III. RESULTS AND DISCUSSION

A. $SrTiO_3$ (100) surface

Figure 1 shows normal-emission spectra of the $SrTiO_3$ (100) surface taken with $h\nu$ between 17 and 36 eV. The

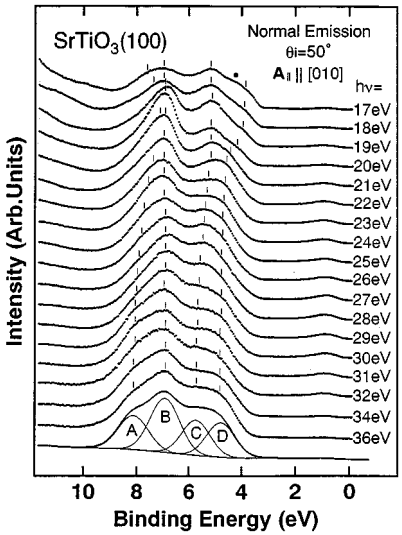

FIG. 1. Normal-emission spectra of the $SrTiO_3$ (100) surface taken with $h\nu$ between 17 and 36 eV and with a light incidence angle of $\theta_i = 50°$. The surface component of the vector potential of incident light $\mathbf{A}_\parallel$ is in the [010] azimuth ($\mathbf{A}_\parallel \parallel [010]$). Verticals in each spectrum indicate peak positions used in the band mapping. The bottom curve is the $h\nu$ = 36-eV spectrum fitted with four Gaussians (see text).

surface component of the vector potential of incident light ($\mathbf{A}_\parallel$) was in the [010] azimuth ($\mathbf{A}_\parallel \parallel [010]$). The valence band between 3 and 9 eV is predominantly derived from O $2p$ and partially from Ti $3d$.[16] Four features in this valence band are observed at ~4.5, 5.5, 7.0, and 8.0 eV labeled A, B, C, and D, respectively. Verticals in Fig. 1 indicate peak positions determined from minimal points of the second derivative of the spectra with respect to the binding energy. In order to confirm the peak positions determined by this method, the ARP spectra were also fitted with four Gaussians. The background was subtracted by the Shirley-type one before the fitting procedure. As an example of the Gaussian fit, the curve fitted with four Gaussians for the $h\nu = 36$ eV ARP spectrum is presented at the bottom of Fig. 1. It is found that the peak positions determined by the second derivative method are in excellent agreement with those by the Gaussian fitting method. One of the prominent features, B, shows a small dispersion about 0.1 eV, with varying $h\nu$ and intensity enhancement is observed near $h\nu \sim 20$ eV. Another prominent feature C indicates some energy shift from 5.1 to 5.7 eV with increasing $h\nu$ from 17 eV. Feature A, which is observed as a shoulder at higher binding-energy side of feature B, comes out at 7.2 eV for $h\nu \sim 21$ eV and gradually shifts to 8.1 eV with increasing $h\nu$. Feature D is also observed as a shoulder at lower binding-energy side of feature C, and clearly shifts from 3.9 to 4.8 eV with increasing $h\nu$. Another feature is seen at ~1.0 eV below E_F. This feature arises from the emission caused by some oxygen vacancies near the surface region, as we reported previously.[17]

As shown in Fig. 1, the ARP spectra of the valence band are broad and essentially the same as those in the previous ARP study.[15] In order to estimate the influence of sample temperature on the broadening effect in the valence band of $SrTiO_3$, we measured the angle-integrated photoemission spectra at ~80 and ~300 K.[18] From the comparison between these spectra, it was found that the valence-band spectra of $SrTiO_3$ does not depend much on the sample temperature. This may indicate that the observed broadening effect is caused by an intrinsic electronic effect in $SrTiO_3$. This broadening effect has been pointed out by Tezuka *et al.*[4] based on a comparison between the theoretical and empirical DOS's. The origin of the broadening effect is not clear at present.

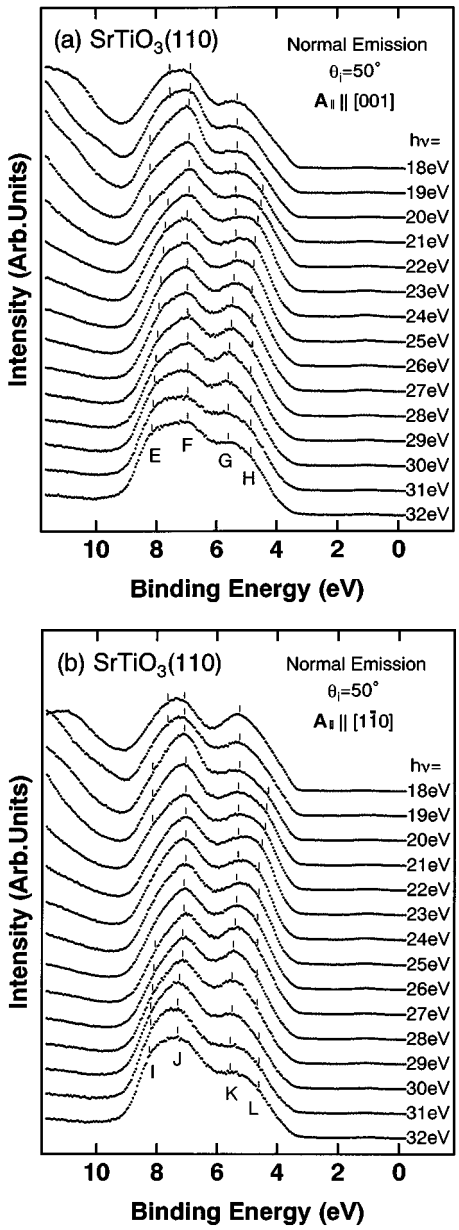

FIG. 2. Normal-emission spectra of the $SrTiO_3$ (110) surface taken with $h\nu$ between 18 and 32 eV. Surface component of the vector potential of incident light $\mathbf{A}_\parallel$ is (a) in the [001] azimuth, and (b) in the $[1\bar{1}0]$ azimuth. Verticals in each spectrum indicate peak positions used in the band mapping.

B. $SrTiO_3$ (110) surface

Figures 2(a) and 2(b) show normal-emission spectra of a $SrTiO_3$ (110) surface taken with $h\nu$ between 18 and 32 eV. $\mathbf{A}_\parallel$ were in the [001] azimuth ($\mathbf{A}_\parallel \parallel [001]$) for Fig. 2(a), and

in the $[1\bar{1}0]$ azimuth ($\mathbf{A}_\parallel \parallel [1\bar{1}0]$) for Fig. 2(b). Verticals in Figs. 2(a) and 2(b) indicate peak positions determined as minimal points of the second derivative of the spectra with respect to the binding energy. Four features in this valence band are observed at ~4.5, 5.5, 7.0, and 8.0 eV labeled *E*, *F*, *G*, and *H* for $\mathbf{A}_\parallel \parallel [001]$, and *I*, *J*, *K*, and *L* for $\mathbf{A}_\parallel \parallel [1\bar{1}0]$. For $\mathbf{A}_\parallel \parallel [001]$, two prominent features *F* and *G* and two shoulder features *E* and *H*, similar to the case of the (100) surface, are seen in Fig. 2(a). Feature *E* appears at ~23 eV and monotonically shifts from 7.6 to 8.2 eV with increasing $h\nu$. Feature *F* has little shifts with changing $h\nu$, and some intensity enhancement is observed near $h\nu \sim 20$ eV. Feature *G* shows an energy shifts from 5.3 to 5.6 eV by ~0.3 eV with increasing $h\nu$. Feature *H* is observed as a shoulder, and clearly shifts from 4.5 to 4.9 eV with increasing $h\nu$ from 21 eV. For $\mathbf{A}_\parallel \parallel [1\bar{1}0]$, similar to the $\mathbf{A}_\parallel \parallel [001]$ case, two prominent features *J* and *K* and two shoulder features *I* and *L* were shown in Fig. 2(b). Feature *I* is visible only near $h\nu \sim 30$ eV, and shows a slight dispersion from 8.1 to 8.3 eV with increasing $h\nu$ from 30 to 32 eV. Feature *J* shows a small dispersion with respect to $h\nu$. Feature *K* shows an energy shift from 5.3 to 5.6 eV by ~0.3 eV with increasing $h\nu$. Feature *L* is observed as a shoulder of feature *K*, and shifts from 4.3 to 4.6 eV with increasing $h\nu$ from 20 eV. Another feature is observed as a shoulder near $h\nu = 20$ eV for $\mathbf{A}_\parallel \parallel [1\bar{1}0]$ and [001], and stays at ~8.2 eV.

C. Band mapping

In the direct transition model, the valence-band features in the normal-emission spectra in Figs. 1 and 2 are related to transitions involving the initial states lying on the Γ-Δ-*X* and Γ-Σ-*M* lines of the bulk Brillouin zone for the (100) and (110) surfaces, respectively. In order to map these bands from the observed ARP spectra, we assume direct transitions into a free-electron-like final state of the form. $E(k_\perp) = (h^2k_\perp^2/8\pi^2m^*) - V_0$, where m^* is the effective mass of electrons, V_0 is the inner potential referred to E_F, and $k_\perp$ is the component of the wave vector of the outgoing photoelectron normal to the surface. V_0 and m^* have been decided as empirical adjustable parameters to obtain the initial-state dispersion which is symmetric about the Brillouin-zone boundary. Using $V_0 = 12.0$ eV and $m^* = 1.52m_e$ for the (100) surface, and $m^* = 1.10m_e$ for the (110) surface, where m_e is the free-electron mass, the empirical band structure along the Δ line (circles) and Σ line (squares for $\mathbf{A}_\parallel \parallel [001]$ and triangles for $\mathbf{A}_\parallel \parallel [1\bar{1}0]$) is shown in Fig. 3. The band structure calculated by Takegahara (solid lines) using the augmented-plane-wave (APW) method with muffin tin and the local-density approximation (LDA) is included for comparison.[9] The binding energy of the calculated band structure is referenced to the valence-band maximum.

First we will discuss the band structure along the Δ line. As shown in Fig. 3, the empirical band structure along the Δ line is determined throughout the bulk Brillouin zone. In a previous ARP study,[15] Brookes *et al.* determined the band structure for only half of the Δ line near the *X* point. They reported that final-state effects appear at $h\nu \leqslant 23$ eV. However, we were able to determine the band structure without suffering from such effects. In the second derivative curve of

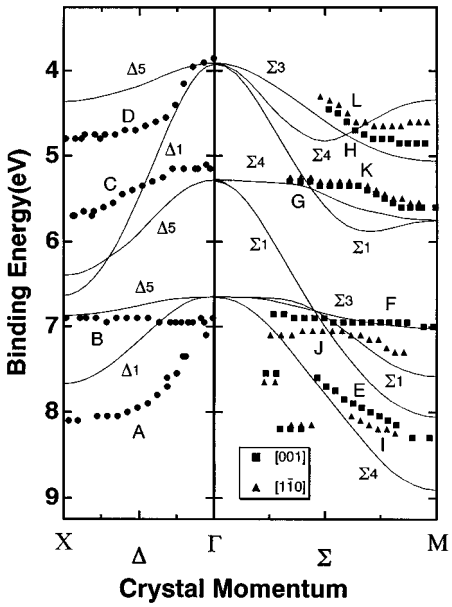

FIG. 3. Empirical valence-band structure along the Δ line and Σ line in the bulk Brillouin zone. Circles are deduced from Fig. 1 for the (100) surface. Squares and triangles are deduced from Fig. 2(a) ($\mathbf{A}_\parallel \parallel [001]$) and (b) ($\mathbf{A}_\parallel \parallel [1\bar{1}0]$) for the (110) surface, respectively. For comparison, the band structure calculated by Takegahara (Ref. 9) using the APW method is included (solid lines).

the $h\nu = 17$-eV spectrum, another feature which deviates from the band structure appeared at ~4.3 eV (marked by a solid circle in Fig. 1). This peak may correspond to the manifestation of the final-state effects. For normal emission from the (100) surface, initial states with symmetries of Δ_1 and Δ_5 should be observed according to the dipole selection rule for the cubic crystals.[19] The band theory has suggested that the valence band of $SrTiO_3$ along the Δ line consists of two Δ_1 bands and three Δ_5 bands, as shown in Fig. 3. From a comparison with the Takegahara's calculation,[9] three features *A*, *B*, and *C* are assigned to the Δ_1 band on the higher binding-energy side (hereafter, called higher Δ_1 band, and so on), the higher Δ_5 band and the middle Δ_5 band in the calculated band structure, respectively. These assignments agree with those of the previous ARP study by Brookes *et al.*[15] They assigned feature *D* to the lower Δ_1 band.[15] In order to maximize the overlap between their empirical bands and the calculated bands by Wolfram, Kraut, and Morin,[7] they shifted rigidly the higher Δ_1 and Δ_5 bands toward higher binding energy by ~1.0 eV.[15] This energetic modification was made on the grounds that the O $2p$ crystal-field splitting in the calculation by Wolfram, Kraut, and Morin was underestimated. However, the O $2p$ crystal-field splitting affects not only the shift of the higher Δ_1 and Δ_5 bands but also the width of each band: based on the band calculation by the simple linear combination of atomic orbitals (LCAO) method,[20] the bandwidths of the middle Δ_5 and the lower Δ_1 bands are in proportion to the O $2p$ crystal-field splitting. That is, the bandwidths of these bands after the modification of the O $2p$ crystal-field splitting are expected to be 50% larger than that before the modification. Therefore, it is not feasible to assign feature *D* to the lower Δ_1 band in the calculated band structure. On the other hand, the O $2p$

crystal-field of Takegahara's band structure[9] is qualitatively in agreement with that of our empirical band structure. Therefore, we compared our empirical band structure with the calculated band structure of Takegahara as shown in Fig. 3: the observed bandwidth of feature D ($\sim$1.0 eV) does not agree with that of the calculated lower Δ_1 band ($\sim$2.7 eV), but roughly with that of the calculated lower Δ_5 band ($\sim$0.5 eV). Therefore, feature D can be assigned to the lower Δ_5 band. Here the reason why the lower Δ_1 band is hardly observed in our ARP spectra may be explained as follows: the lower Δ_1 band with a large dispersion of 2.7 eV is expected to have a smaller DOS as compared with other bands. Hardman *et al.*[11] pointed out some bands with large dispersion in the TiO_2 band calculation as ''missing bands'' for the same reason.

For normal emission from the (110) surface, initial states with symmetries of Σ_1, Σ_3 for $\mathbf{A}_\parallel \parallel [001]$ and of Σ_1, Σ_4 for $\mathbf{A}_\parallel \parallel [1\bar{1}0]$ should be observed according to the selection rule.[19] The valence band along the Σ line consists of three Σ_1 bands, one Σ_2 band, two Σ_3 bands, and three Σ_4 bands in the band theory. Since the Σ_2 band cannot be observed under our experimental geometry, the calculated bands with only other Σ_1, Σ_3, and Σ_4 symmetries are shown in Fig. 3. From a comparison with the calculation, two features E and H for $\mathbf{A}_\parallel \parallel [001]$ can be assigned to the higher Σ_1 band and the lower Σ_3 band, respectively. However, feature F cannot be clearly assigned since the higher Σ_3 band is located near the middle Σ_1 band. For $\mathbf{A}_\parallel \parallel [1\bar{1}0]$, three features I, J, and L are possibly assigned to the higher Σ_1 band, the middle Σ_1 band, and the lower Σ_4 band, respectively. Concerning the two remaining features, G for $\mathbf{A}_\parallel \parallel [001]$ and K for $\mathbf{A}_\parallel \parallel [1\bar{1}0]$, there are two candidates for the origin. First, these features may simply be explained by the band picture. That is, as shown in Fig. 3, it is considered that feature G is considered to be composed by the lower Σ_1 band, and feature K by not only the lower Σ_1 band but also the middle Σ_4 band. In the spectra of $h\nu = 18$ eV of Figs. 2(a) and 2(b), the relative intensity of feature K compared to feature J is enhanced compared with that of feature G to feature F. The observed relative intensity variation is expected to be induced by a symmetry difference between these features, namely by the additional Σ_4 symmetry of feature K compared to feature G. Second, features G and K may be ascribed to surface resonance. On the TiO_2 (100) surface, a surface resonance is observed at $\sim$5.5 eV below E_F.[11] The intensity of the surface resonance is comparable with that of other bulk features. According to a calculation for the TiO_2 surface by Munnix and Schmeits,[21] the surface resonance is derived from O $2p$, and arises from the change of coordination of the terminating O atoms. This situation in the TiO_2 (100) surface may be realized in the $SrTiO_3$ (110) surface. On the whole, our empirical band structure is qualitatively in overall agreement with the calculated one except for some discrepancy in energy near the X and M points.

We are pleased to thank the staff of the Photon Factory at the National Laboratory for High Energy Physics for excellent support. This work has been performed under the approval of the Photon Factory Program Advisory Committee (Proposal Nos. 91-142 and 93G133), and was partially supported by NEDO for the R&D of Industrial Science and Technology Frontier Program.

[1] M. Cardona, Phys. Rev. **140**, A651 (1965).
[2] F. L. Battye, H. Höchst, and A. Goldmann, Solid State Commun. **19**, 269 (1976).
[3] B. Reihl, J. G. Bednorz, K. A. Müller, Y. Jugnet, G. Landgren, and J. F. Morar, Phys. Rev. B **30**, 803 (1984).
[4] Y. Tezuka, S. Shin, T. Ishii, T. Ejima, S. Suzuki, and S. Sato, J. Phys. Soc. Jpn. **63**, 347 (1994).
[5] T. F. Soules, E. J. Kelly, D. M. Vaught, and J. W. Richardson, Phys. Rev. B **6**, 1519 (1972).
[6] L. F. Mattheiss, Phys. Rev. B **6**, 4718 (1972).
[7] T. Wolfram, E. A. Kraut, and F. J. Morin, Phys. Rev. B **7**, 1677 (1973).
[8] P. Pertosa and F. M. Michel-Calendini, Phys. Rev. B **17**, 2011 (1978).
[9] K. Takegahara, J. Electron Spectros. Relat. Phenom. **66**, 303 (1994).
[10] S. Hüfner, *Photoelectron Spectroscopy*, Springer Series in Solid-State Science Vol. 82 (Springer-Verlag, Berlin, 1995), p. 297.
[11] P. J. Hardman, D. N. Raikar, C. A. Muryn, G. van der Laan, P. L. Wincott, G. Thornton, D. W. Bullett, and P. A. D. M. A. Dale, Phys. Rev. B **49**, 7170 (1994).
[12] K. Siratori, S. Suga, M. Taniguchi, K. Soda, S. Kimura, and A. Yanase, J. Phys. Soc. Jpn. **55**, 690 (1986).
[13] Z.-X. Shen, C. K. Shih, O. Jepsen, W. E. Spicer, I. Lindau, and J. W. Allen, Phys. Rev. Lett. **64**, 2442 (1990); Z.-X. Shen, J. W. Allen, P. A. P. Lindberg, D. S. Dessau, B. O. Wells, A. Borg, W. Ellis, J. S. Kang, S.-J. Oh, I. Lindau, and W. E. Spicer, Phys. Rev. B **42**, 1817 (1990).
[14] H. Kuhlenbeck, G. Odörfer, R. Jaeger, G. Illing, M. Menges, Th. Mull, H.-J. Freund, M. Pöhlchen, V. Staemmler, S. Witzel, C. Scharfschwerdt, K. Wennemann, T. Liedtke, and M. Neumann, Phys. Rev. B **43**, 1969 (1991).
[15] N. B. Brookes, D. S.-L. Law, T. S. Padmore, D. R. Warburton, and G. Thornton, Solid State Commun. **57**, 473 (1986).
[16] R. Courths, B. Cord, and H. Saalfeld, Solid State Commun. **70**, 1047 (1989).
[17] Y. Aiura, H. Bando, Y. Nishihara, Y. Haruyama, T. Komeda, S. Kodaira, Y. Sakisaka, T. Maruyama, and H. Kato, in *Advances in Superconductivity VI*, edited by T. Fujita and Y. Shiohara (Springer, Tokyo, 1994), p. 983.
[18] The angle-integrated photoemission experiments were carried out in a conventional UHV system with the hemispherical electrostatic analyzer (VG) using a He discharge lamp. The total instrumental energy resolutions were $\sim$80 and $\sim$120 meV FWHM at $\sim$80 and at $\sim$300 K, respectively.
[19] J. Hermanson, Solid State Commun. **22**, 9 (1977).
[20] W. A. Harrison, *Electronic Structure and the Properties of Solids: The Physics of the Chemical Bond* (Freeman, San Francisco, 1980), Chap. 19.
[21] S. Munnix and M. Schmeits, Phys. Rev. B **30**, 2202 (1984).